Fuel 155 (2015) 77–85

Contents lists available at ScienceDirect

Fuel

journal homepage: www.elsevier.com/locate/fuel

Surface characterization of rice husk bio-char produced by liquefaction and application for cationic dye (Malachite green) adsorption

Lijian Leng [a,b], Xingzhong Yuan [a,b,*], Guangming Zeng [a,b], Jianguang Shao [a,b], Xiaohong Chen [c], Zhibin Wu [a,b], Hou Wang [a,b], Xin Peng [a,b]

[a] College of Environmental Science and Engineering, Hunan University, Changsha 410082, PR China
[b] Key Laboratory of Environment Biology and Pollution Control, Hunan University, Ministry of Education, Changsha 410082, PR China
[c] School of Business, Central South University, Changsha 410083, PR China

HIGHLIGHTS

- Rice husk bio-char was effective on Malachite green removal from aqueous.
- Malachite green adsorption capacity depended strongly on carboxylic groups.
- Electrostatic attraction was believed to be the major adsorption mechanism.
- Bio-char produced with ethanol at low temperature favored Malachite green adsorption.

GRAPHICAL ABSTRACT

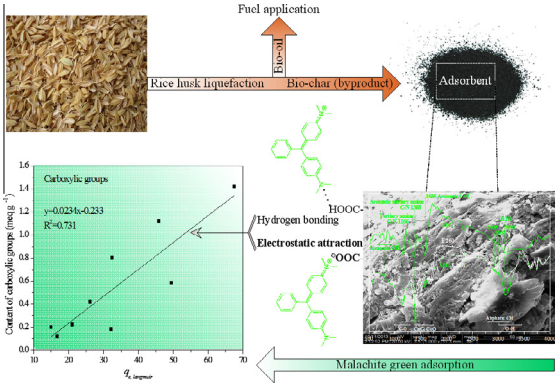

ARTICLE INFO

Article history:
Received 25 January 2015
Received in revised form 3 April 2015
Accepted 11 April 2015
Available online 20 April 2015

Keywords:
Rice husk
Liquefaction byproduct
Bio-char
Malachite green
Oxygen-containing functional group

ABSTRACT

The byproduct (bio-char) from liquefaction of rice husk with water, water/ethanol (V/V, 5:5), or ethanol as the solvent at 260–340 °C was characterized in terms of its elemental composition, thermogravimetric characteristics, surface area and pore size distribution, morphology, and oxygen-containing functional group composition. The liquefaction bio-char produced with water (WBC) or water/ethanol (WEBC) as the solvent was rich in phenolic groups and bio-char with ethanol as the solvent (EBC) was rich in carboxylic and lactonic groups. Dye adsorption results indicate that the liquefaction bio-char was effective on cationic Malachite green (MG) removal from aqueous solution, but was not on anionic Methyl orange. It was also shown that the MG adsorption behaviors depended strongly on the oxygen-containing functional groups especially carboxylic groups. EBC (adsorption capacities, 32.5–67.6 mg g^{-1}) was more effective on MG adsorption than WBC and WEBC. The adsorption equilibrium, kinetic, thermodynamic, and mechanism analysis indicate that electrostatic attraction was the major force for MG adsorption onto the bio-char. The MG adsorption kinetic fitted Pseudo-second-order model well and the isotherm can be well described by Langmuir, Freundlich, and Temkin models. The RH bio-char (byproduct) produced from

Abbreviations: RH, rice husk; WBC, rice husk bio-char produced by liquefaction with water as the solvent; WBC260, rice husk bio-char produced by liquefaction with water as the solvent at 260 °C; WEBC, rice husk bio-char produced by liquefaction with water/ethanol (V/V, 5:5) as the solvent; WEBC260, rice husk bio-char produced by liquefaction with water/ethanol (V/V, 5:5) as the solvent at 260 °C; EBC, rice husk bio-char produced by liquefaction with ethanol as the solvent; EBC260, rice husk bio-char produced by liquefaction with ethanol as the solvent at 260 °C; MG, Malachite green; MO, Methyl orange; MB, methylene blue; TGA, thermogravimetric analysis; FT-IR, Fourier transform infrared; XPS, X-ray photoelectron spectrometer; SEM, scanning electron microscope; BET, Brunauer–Emmett–Teller; IUPAC, International Union of Pure and Applied Chemistry.

* Corresponding author at: College of Environmental Science and Engineering, Hunan University, Changsha 410082, PR China. Tel.: +86 731 88821413; fax: +86 731 88823701.
E-mail address: yxz@hnu.edu.cn (X. Yuan).

http://dx.doi.org/10.1016/j.fuel.2015.04.019

liquefaction could be served as potential low-cost adsorbent for cationic dye removal from aqueous solution.

1. Introduction

Dyes, representing an important class of pollutants among others, are often discharged in the form of colored wastewater by textile industries, pulp mills, and dye manufacturing industries. Many of these colored compounds are toxic, posing great potential threat to aquatic lives and human beings [1]. Adsorption is one of the most effective methods for dye removal from aqueous solutions [2,3]. Activated carbon is currently the most commonly and widely used adsorbent for the adsorption of pollutants such as dye from liquid effluents, due to its large surface area, multiporous structure, and thermo-stability [2,4].

However, due to the rising production costs of commercially available activated carbon, researchers are seeking the feasibility of using various low-cost adsorbents derived from natural materials, industrial solid wastes, agricultural byproducts, and biosorbents as the precursors [3,5]. Among these precursors, agricultural byproduct rice husk (RH) has received rising attention with the advantages of low cost, inherited prominent properties to be used as precursor, and the abundance and availability especially in developing countries [6]. RH based adsorbents have been reported to have good performances for removal of a wide variety of organic [7,8] and inorganic pollutants [9] dissolved in aqueous media. These RH based adsorbents were most commonly produced by physical and chemical activation [4,8].

Recently, liquefaction, a low temperature (250–350 °C) and high pressure (5–20 MPa) process with solvent participation (including hydrothermal liquefaction which use water as the solvent), which was commonly used for bio-oil (main product) production, has been taken into account for potential effective adsorbent (bio-char) production [10,11]. Specifically, the RH is one of the commonly used raw material for bio-oil production by liquefaction [12], and the byproduct (bio-char) produced by hydrothermal liquefaction (solvent: water) from RH was proven to be effective on its adsorption of lead, copper, and phenol, especially when the char was activated [10,13]. Liu et al's study also showed that bio-char produced by hydrothermal liquefaction had better performance on copper removal than pyrolysis bio-char because of the abundant functional groups on the surface of liquefaction bio-char [11]. These prominent performances might most probably due to the insightful advantageous surface chemistry rather than the porosity. Liquefaction bio-char is often produced with very small surface area and pore volume, but is rich in surface functional groups [11,14]. Surface functional groups can provide possible affinities for the target pollutants and the favorable surface chemistry could be of greater important than a high porosity [15]. Note liquefaction bio-char was found to be abundant in oxygen-containing functional groups such as hydroxyl and carboxyl groups [11,14]. These functional groups could afford primary adsorptive forces between the adsorbent and cationic adsorbate. Liquefaction bio-char (byproduct) might be developed to be effective on removal of cationic organic or inorganic compounds.

Liquefaction solvent and temperature could have drastic impact on the content profile of oxygen-containing functional groups on liquefaction bio-char, but few studies have been done. In this study, RH based bio-char, the byproduct produced from liquefaction with different solvent at different temperature in Ref. [12], was characterized and applied for dye removal from aqueous solution in order to find an appropriate solvent and temperature for the production of effective adsorbent, and to gain an insight into the adsorption mechanism of the bio-char. It is expected that this work will enhance the utilization of the byproduct (bio-char) of liquefaction and promote the development of liquefaction in industry.

2. Materials and methods

2.1. Bio-char production

RH bio-char (byproduct) was produced with water, 5:5 water/ethanol, or ethanol as the solvent at 260–340 °C [12]. Briefly, thermochemical liquefaction of RH was carried out in a 500 mL autoclave reactor (GSHA-0.5, China). In each experiment, the reactor was loaded with about 8.0 g RH and 100 mL solvent (water, ethanol, or water/ethanol mixture of ratio 5:5), with temperature then raised to the desired levels (260, 300, or 340 °C) and maintained for 20 min [12]. Afterwards, the reactor was cooled down to the room temperature. Then the solid/liquid products were rinsed by washing the autoclave with water and diethyl ether, separately, and then filtered under vacuum to separate the solid and liquid products. The filtrate was further evaporated to obtain the main product bio-oil, which was reported in detail in Ref. [12]. The solid product (byproduct bio-char) was recovered and dried in an oven at 105 °C for 24 h and then ground to less than 75 μm and kept in a desiccator for use. Bio-char obtained with water (WBC), ethanol (EBC), and 5:5 water/ethanol (WEBC) as the solvent at 260 °C was labeled WBC260, WEBC260, and EBC260, respectively. In the same way, bio-char produced at 300 °C (340 °C) was labeled WBC300 (WBC340), WEBC300 (WEBC340), and EBC300 (EBC340), respectively.

2.2. Characterization of samples

The elemental (C, H, N) analysis was performed with an Elemental Analyzer (Elementar, Vario EL III, Germany). The pH of samples was measured in a suspension of 1:10 sample/deionized water using a combination electrode after 1 h shaken [16]. The measurement of the point of zero charge (pH_{PZC}) of the bio-char was determined according to Ref. [14]. Briefly, the pH of 20 mL 0.01 M NaCl solution in a closed vessel was adjusted to a value from 3 to 10 with 0.1 M HCl or 0.1 M NaOH. Then, 0.10 g bio-char was added and the solution pH after 24 h of agitation was measured. The point of zero charge is the point where the curve $\Delta pH = pH\ (final) - pH\ (initial) = 0$ [14].

The oxygenated acidic groups of samples were determined using the Boehm's titration [17,18]. Prior to measurement, the bio-char samples were equilibrated with dilute HCl solution (pH 2) for 3 d, followed by washing with deionized water until no Cl^- existed in effluent as detected by $AgNO_3$ [19]. A dried char sample (0.2 g) was mixed with 25 mL of the 0.05 M solution of sodium bicarbonate ($NaHCO_3$), sodium carbonate (Na_2CO_3), sodium hydroxide (NaOH), and sodium ethoxide (C_2H_5ONa). The sample suspensions were shaken at a speed of 150 rpm at 25 °C for 48 h. The excess of base in 5 mL of the filtrate was titrated with 0.05 M HCl. Total acidity and the contents of oxygen-containing functional groups were calculated on the basis of assuming that $NaHCO_3$ neutralizes carboxyl groups only, Na_2CO_3 neutralizes carboxyl and lactonic groups, NaOH neutralizes carboxyl, lactonic, and

phenolic groups, $NaOC_2H_5$ neutralizes all acidic groups including carboxyl, lactonic, phenolic, and carbonylic groups [16,17,19]. Each sample was analyzed twice.

Thermogravimetric analysis (TGA) of bio-chars was performed with an integrated thermal gravimetric analyzer (EXSTAR, TG/DTA 7300, Japan) by heating from room temperature to 800 °C with a constant heating rate of 10 °C min^{-1} at nitrogen (purity of 99.99%) flow rate of 100 mL min^{-1}. The functional groups and surface properties of samples were examined by Fourier transform infrared (FT-IR) spectra (WQF-410, China) at room temperature in the wavelength range of 400–4000 cm^{-1} and X-ray photoelectron spectrometer (XPS) techniques (Thermo Fisher 158 Scientific-K-Alpha 1063, UK) with high-resolution spectra binding energies. The surface morphology was studied by scanning electron microscope (SEM, FEI-Quanta200, Holland). The Brunauer–Emmett–Teller (BET) specific surface area and pore size were determined with a N_2 adsorption–desorption isotherm measured at 77 K using a Quantasorb SI instrument (Quantachrone, USA).

2.3. Batch sorption experiment

Typical anionic Methyl orange (MO) and cationic Malachite green (MG) dyes were selected for bio-char adsorption experiment. The detailed information of MO and MG used in this study is given in Table S1. The effect of some important parameters on removal of MG studied include adsorbent dosage (0.25–2.0 g L^{-1}), contact time (1–720 min), pH (3–10, adjusted with 0.1 M HCl or 0.1 M NaOH), temperature (30–60 °C), and initial adsorbate concentration (20–120 mg L^{-1}).

For each adsorption study, a 20 mL volume of a dye solution of known initial concentration was mixed with a known amount of adsorbent. The resulting suspension was then shaken at a constant speed of 150 rpm until equilibrium. After the attainment of sorption equilibrium, samples were centrifuged at 8000 rpm and the supernatant were analyzed using an Ultraviolet–Visible (UV–Visible) spectrophotometer (Shimadzu, Model UV-200S, Japan) at wavelength values of 510 and 618 nm for MO and MG, respectively.

The adsorption capacity (q_e, mg g^{-1}) was calculated from the difference between the initial and equilibrium dye concentrations according to the following equation:

$$q_e = V(C_o - C_e)/m \quad (1)$$

where C_o is the initial dye concentration (mg L^{-1}), C_e is the equilibrium dye concentration (mg L^{-1}), V is the volume of the liquid phase (mL) and m is the mass of the adsorbent (mg).

The adsorption experiments were repeated in triplicate and the average values were reported with differences generally <5%.

2.4. Theories

In order to analyze and design an adsorption process, different adsorption isotherm and kinetic models, and thermodynamic equations were applied to fit the experimental data to find adequate models to predict isotherm, kinetic, and thermodynamic data. The different theoretical models or equations are tabulated in Table S2.

3. Results and discussions

3.1. Characterization of liquefaction bio-char

3.1.1. TGA analysis

The RH bio-char yields during liquefaction were in the sequence: EBC (48.8% at 260 °C, 41.3% at 300 °C, and 33.6% at 340 °C) > WEBC (25.1% at 260 °C, 21.7% at 300 °C, and 22.4% at 340 °C) > WBC (30.2% at 260 °C, 14.8% at 300 °C, and 10.5% at 340 °C), and the increasing liquefaction temperature reduced the bio-char yields [12]. As seen in Fig. S1, Weight loss of the RH sample mainly occurred between 200 and 500 °C, and the amount of solid residue left after 800 °C was around 21.42%. The reaction zone (200–418 °C) mainly corresponded to hemicellulose–cellulose degradation while the zone (418–700 °C) mainly corresponded to lignin decomposition [20]. The weight loss of the liquefaction bio-char was mainly between 270 and 500 °C. The obviously higher weight loss of RH between 200 and 350 °C than those of liquefaction bio-chars suggests that the hemicellulose–cellulose between 200 and 350 °C would have reacted with the solvent (water and/or ethanol) to produce bio-oil, water, and gas product after liquefaction. The high molecular hemicellulose–cellulose and most of the lignin were resided to produce the bio-chars after the reaction.

3.1.2. Proximate analysis and elemental compositions

As shown in Table 1, the ash yields of the liquefaction bio-chars were relatively higher than that of RH due to that RH lost large part of its volatile compound during liquefaction. The relative element contents showed the loss of oxygen and the enrichment of carbon, which were resulted from the condensation and carbonization reactions of raw RH, respectively. The mole ratios of H/C and O/C of bio-chars decreased obviously compared to those of RH, indicating the involvement of demethylation (loss of CH_3) and decarboxylation (loss of CO_2) during liquefaction, respectively [21,22]. At the same time, oxygen-containing bio-oil components like phenolic compounds, ketones, and esters were formed [12,22].

3.1.3. Surface area and morphology

As shown in Table 2, the surface areas of bio-chars were extremely low (8.2–21.7 m^2 g^{-1}) although it was relatively higher than that of RH. The surface areas obtained here were comparable to those of liquefaction bio-chars obtained in other studies [10,14]. The low surface area and pore volume may be related to pore blockage due to the presence of organic matter [16]. Among these bio-chars, WEBC260 had relatively higher surface area and pore volume than those of EBC260 and WBC260, respectively. EBC260 had a lower pore volume than WBC260 although its surface area was a bit higher. Nevertheless, both RH and its bio-chars were mesoporous material because their average pore size fall between 2 and 50 nm (for mesopores) as classified by the International Union of Pure and Applied Chemistry (IUPAC) [23]. Additionally, it may be supposed that these bio-chars belong to the Type IV adsorption isotherms and the hysteresis loop observed in the isotherms (Fig. 1) was associated with capillary condensation taken place in the mesopores of the bio-chars [14,23]. By possessing small dimensions, the bio-char may provide a good approximation of the entire surface area available for the adsorption of the lower weight molecular compounds [24].

Table 1
Proximate analysis and elemental compositions of rice husk and its liquefaction bio-chars.

Sample	pH	Ash[a] (%)	Elemental composition[b] (%)					
			C	H	O [c]	N	H/C [d]	O/C [d]
RS	5.62	14.77	43.06	6.08	46.60	4.26	1.69	0.81
WBC260	6.73	24.54	69.15	6.99	19.35	4.51	1.21	0.21
WEBC260	6.50	25.22	51.74	5.57	37.63	5.07	1.29	0.55
EBC260	6.33	28.25	58.69	6.94	29.65	4.72	1.42	0.38

[a] Ash yields are on a dry basis.
[b] Elemental composition is on a daf basis.
[c] By difference, O = 100 – C—H—N.
[d] The mole ratio of H to C (H/C) and O to C (O/C).

Table 2
BET and XPS analyses and Boehm's titration of rice husk and its liquefaction bio-chars.

Sample	BET analysis			XPS analysis			
	Surface area ($m^2\ g^{-1}$)	Average pore size (d, nm)	V_{total}, (P/P_o = 0.99) ($cm^3\ g^{-1}$)	C1s(1) C—C/C—H_X (eV/%)	C1s(2) C—O (eV/%)	C1s(3) C=O (eV/%)	C1s(4) O=C—O (eV/%)
RS	1.5	7.1	0.002	284.7/77.8	286.3/7.0	287.1/7.4	288.2/7.8
WBC260	8.2	21.7	0.044	284.6/62.4	286.3/25.8	287.1/8.8	288.4/3.0
WEBC260	21.7	18.8	0.102	284.3/53.3	286.3/43.1	287.1/0.2	288.5/3.4
EBC260	9.2	8.0	0.018	284.7/82.5	286.1/1.5	287.1/5.8	288.2/10.2

Sample	Oxygen-containing functional groups ($meq\ g^{-1}$)				Total acidity	pH_{PZC}
	Carboxylic	Lactonic	Phenolic	Carbonylic		
RS	1.26	0.25	0.94	0.67	3.12	–
WBC260	0.18	0.22	1.25	0.56	2.21	6.64
WEBC260	0.58	0.14	2.20	0.00	2.92	6.52
EBC260	1.42	0.68	0.32	0.25	2.67	6.40
WBC300	0.12	0.26	0.62	0.15	1.15	6.75
WEBC300	0.42	0.26	0.82	0.12	1.62	6.61
EBC300	1.12	0.48	0.32	0.40	2.32	6.57
WBC340	0.20	0.42	0.50	0.04	1.16	7.06
WEBC340	0.22	0.32	0.78	0.04	1.36	6.66
EBC340	0.80	0.56	0.25	0.36	1.97	6.65

It is shown in Fig. S2 that noticeable structural changes had taken place during the liquefaction process. The raw RH had relatively smooth surface, while the bio-chars had rough surface with porous structure on the surface particularly for WBC260 and WEBC260. The sizes of cavities in particles of WBC260 and WEBC260 were larger and cell walls were thinner compared to the EBC260, which was in accordance with the pore size results from BET analysis. The changing morphological structure of the bio-chars compared to RH indicates that the chemical reactions occurred with water or water/ethanol as solvent might be more intense than those with ethanol. Thus, liquefaction with water or water/ethanol as solvent resulted in lower bio-char yields than with ethanol as reported in Ref. [12].

3.1.4. Boehm titration

Table 2 presents the contents of total acidity and oxygen-containing functional groups from the Boehm's titration. The raw RH was abundant in oxygen-containing functional groups like carboxylic, phenolic, and carbonylic groups, while WBC and WEBC were rich in phenolic groups, and EBC was rich in carboxylic and lactonic groups. Part of the carboxylic and carbonylic compounds in RH might have reacted with water to produce the phenolic compounds, and thus phenolics dominated bio-oil was obtained when water was used as the solvent [12]. However, when ethanol was used as the solvent, carboxylic compounds would be easier to react with ethanol and promote the production of esters. Thus, higher contents of esters were found in bio-oil produced with ethanol as the solvent [12]. In addition, the increase of liquefaction temperature had a negative effect on carboxylic and phenolic groups. That is to say, the increasing reaction temperature might accelerate the reaction between carboxylic (phenolic) compounds of RH and the solvent water and/or ethanol.

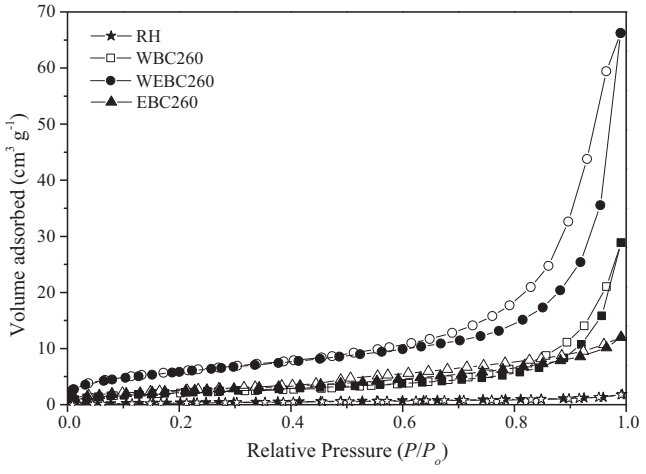

Fig. 1. Nitrogen adsorption–desorption isotherms of rice husk and its liquefaction bio-chars.

3.1.5. XPS analysis

XPS was performed on representative bio-chars (Fig. S3 and Table 2). Deconvolution of the C1s peak for both RH and its bio-chars showed the presence of more than one peak, corresponding to different carbon-based functional groups. The main peak at 284.3–284.7 eV was likely to be a graphitic structure related to C—C/C—H_X [16,25]. The other peaks at around 286.1–286.3, 287.1, and 288.2–288.5 eV can be presumably attributed to C—O (alcohol and/or ether), C=O (carbonyl), and O=C—O (carboxylic acid and/or ester), respectively [16,25]. Liquefaction with water and water/ethanol as the solvent caused a reduction in the C—C/C—H_X peak from 77.8% (RH) to 62.4% (WBC260) and 53.3% (WEBC260), respectively, indicating the loss of volatile compounds and a resultant increase of surface hydrophobicity [16]. An increment of C—C/C—H_X peak (from 77.8% to 82.5%) was seen when ethanol was used as the solvent, resulting in an increasing surface hydrophilicity of EBC260. The peek areas of C—O, C=O, and O=C—O in raw RH were almost in a comparable level. However, the C=O and O=C—O contents of WBC and WEBC were reduced and C—O increased, while those of EBC had opposite trends. The XPS analysis was found to be a well verification of the Boehm's titration results in Section 3.1.4.

3.1.6. FT-IR analysis

As shown in Fig. S4(a), several structural differences between RH and bio-chars can be observed from the FT-IR spectra. The band in the range of 3000–3445 cm^{-1} represents the O—H stretching vibration [26]. The peaks at 2925 cm^{-1}, 2858 cm^{-1}, and 1455 cm^{-1} were assigned to —CH_2 groups [26]. The bands at 1512 cm^{-1} and 1649 cm^{-1} represent C=C stretching vibration of lignin and C=O stretching, respectively [26]. The bands at 1159 cm^{-1} and 1041 cm^{-1} can be assigned to the alcohol C—O

and C—O—C of cellulose [26]. While the band at 1396 cm^{-1} can be assigned to carboxylate groups [27,28]. The changes in bands in the range of 1000–1400 cm^{-1} (C—O) and the band at 1649 cm^{-1} (C=O) indicate that the oxygen-containing functional groups might have experienced some chemical reactions during liquefaction as also identified in the Boehm's titration and XPS studies. The presence of aromatic C—H (802 cm^{-1}) on the surface of bio-chars suggests the involvement of condensation during the liquefaction.

When comparing EBC260-$NaHCO_3$ ($NaHCO_3$ neutralizes carboxyl groups only) to EBC260 (Fig. S4(b)), it is suggested that the bands at 1602 and 1649 cm^{-1}, 1087 and 1115 cm^{-1}, and 3124 and 3175 cm^{-1} became weak and can be assigned to C=O, C—O, and O—H of carboxylic compounds, respectively. The bands at 1681 and 1696 cm^{-1} and 802 cm^{-1} also became weak when EBC260-Na_2CO_3 (Na_2CO_3 neutralizes carboxyl and lactonic groups) was compared to EBC260-$NaHCO_3$, and the bands at 1681 and 1696 cm^{-1} can be assigned to C=O of lactonic compounds. The bands at 1018 and 1159 cm^{-1} and 3278 cm^{-1} showed weaken trends when EBC260-NaOH and EBC260-$NaOC_2H_5$ were compared to EBC260-Na_2CO_3, indicating that they may be assigned to C—O and O—H of alcohol and/or phenolic compounds, respectively.

3.2. Adsorption studies

3.2.1. Adsorption of cationic and anionic dyes on bio-chars

Typical cationic (MG) and anionic (MO) dyes were selected as model organic pollutants to test their adsorption potentials by liquefaction bio-char with different characteristics. The adsorption capacities of MG and MO in Fig. 2 indicate that these RH based liquefaction bio-chars were only effective on cationic dye MG removal. Note the MO adsorption capacities of all bio-chars were all below 6 mg g^{-1}, and the liquefaction solvent and temperature differences had negligible effect on adsorption performances, the surface chemistry (the abundance of functional groups) of the chars may be of little meaning for MO removal. Thus, the adsorption of MO might probably be attributed to physical adsorption. Whereas, the liquefaction solvent and temperature differences of the bio-chars drastically affected the adsorption of MG. Specifically, the EBC showed better performances than WBC and WEBC. In addition, the increment of liquefaction temperature resulted in a reduced MG adsorption capacity, which might because of the drastic differences of oxygen-containing functional groups between these bio-chars. EBC260 was found to be the most effective adsorbent for MG removal and its abundance in oxygen-containing functional groups especially the carboxylic groups could probably be the decisive reason [8,29].

In order to obtain an insight into the adsorption mechanism of MG on RH bio-chars, WBC260, WEBC260, and EBC260 were selected for a deep-in adsorption experiment.

3.2.2. The effect of pH

The values of rate constant demonstrate that adsorption strongly depends on pH of solution and the point of zero charge (pH_{pzc}) of adsorbent [30]. As seen in Table 2, the pH_{pzc} of high-temperature bio-chars was higher than the low-temperature ones, which might be due to that low-temperature bio-chars had a greater number of acid oxygen functional groups [30]. The pH (Table 1) of the bio-chars was almost the same as the pH_{pzc}, meaning their advantage of direct use without the adjustment of pH. As seen in Fig. 3, the adsorption capacity of MG at higher pH was higher than that at lower pH, which may be explained by the surface charge of the bio-chars. The surface functional groups (mainly oxygen-containing groups) linked to the H^+ at lower pH, making these groups in-accessible for MG (cationic), while the deprotonation of functional groups such as carboxylic acids at higher pH provided increasing chance for these groups to co-ordinate with MG and resulted in a higher adsorption capacity [10,31]. The deprotonation may become more obvious at pH higher than 7.5 (higher than the pH_{pzc}), especially for WBC260 and WEBC260, which may result from the deprotonation of phenolic compounds. However, the increment of adsorption capacity at pH higher than 9.0 would probably be due to the alkaline fading of MG for that MG turns into a carbinol base at a basic pH (Fig. 3) [32].

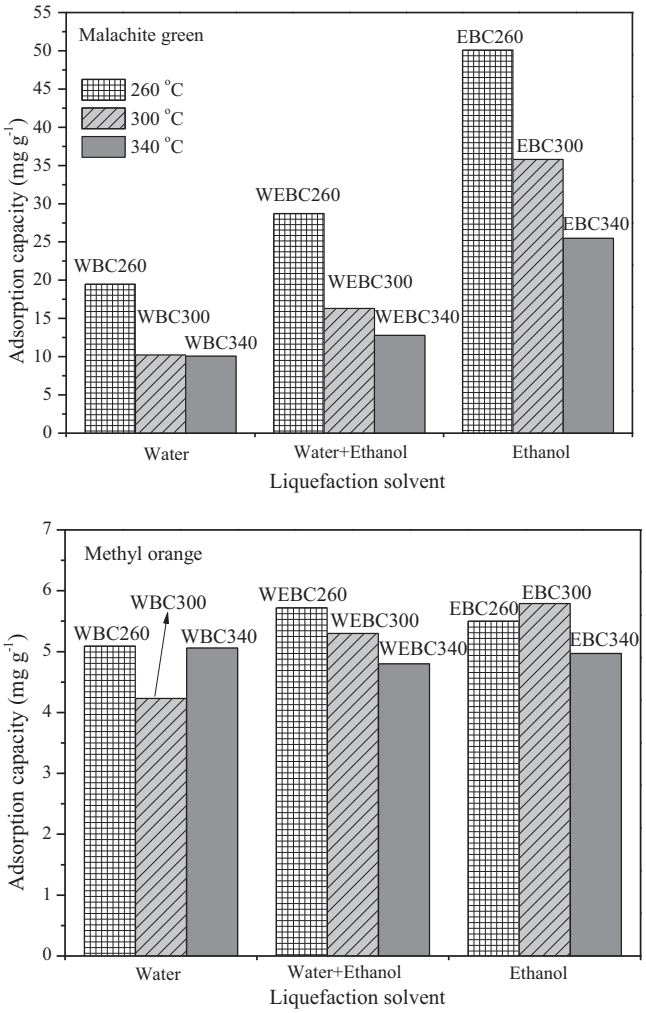

Fig. 2. The adsorption capacities of Methyl orange (MO) and Malachite green (MG) on rice husk bio-char from liquefaction with different surface chemistry (experimental conditions: initial dye concentration: 80 mg L^{-1}, adsorbent dose: 0.5 g L^{-1}, agitation speed: 150 rpm, pH: as received (higher than 6.0, data not show), temperature: 30 °C, contact time: 12 h).

3.2.3. Effect of contact time

The effect of contact time on adsorption of MG was investigated and the results were shown in Fig. 4. The adsorption of MG increased with rise in contact time up to 120 min and the further increase of contact time did not enhance the dye adsorption process obviously. The adsorption rapidly occurred at the initial stage (before 45 min) because of the increment of availability of active binding sites [33]. In the later stage, the adsorption became an attachment-controlled process due to less available sorption sites [33].

3.2.4. Effect of initial dye concentration

As shown in Fig. 5, the adsorption capacity increased with the increasing initial dye concentration and hardly increased at higher concentrations. At lower initial concentrations, the increasing

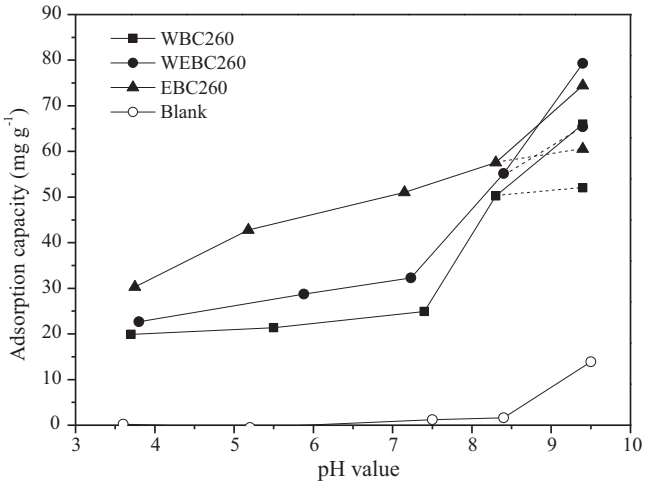

Fig. 3. The effect of pH on the adsorption of Malachite green by bio-chars (experimental conditions: initial dye concentration: 80 mg L^{-1}, adsorbent dose: 0.5 g L^{-1}, agitation speed: 150 rpm, temperature: 30 °C, contact time: 12 h).

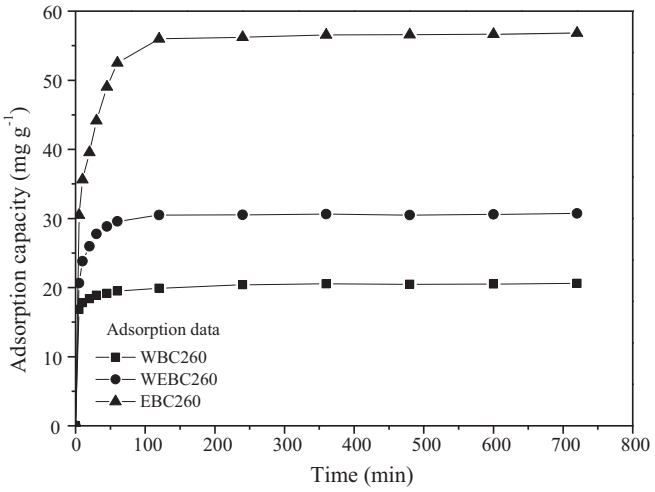

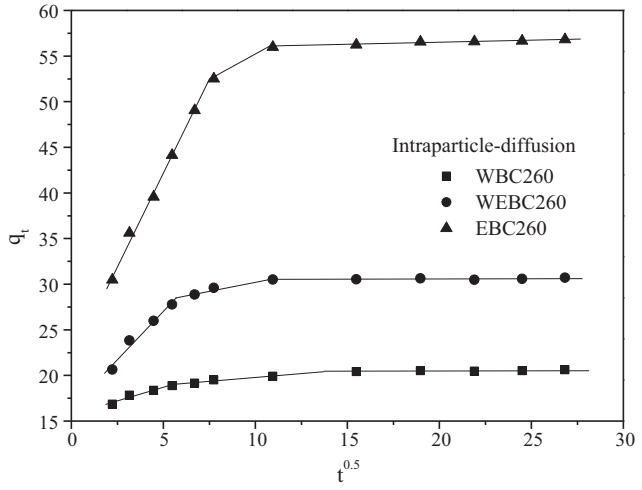

Fig. 4. The effect of contact time on the adsorption of Malachite green by bio-chars and the intraparticle-diffusion modeling plots (experimental conditions: initial dye concentration: 80 mg L^{-1}, adsorbent dose: 0.5 g L^{-1}, agitation speed: 150 rpm, pH: as received, temperature: 30 °C, contact time: 12 h).

concentration acted as increasing driving force for MG to overcome all mass transfer resistances between the aqueous and solid phase [33,34], providing a higher contact probability between bio-chars and MG, and resulted to an increasing adsorption capacity [10,33]. At relatively higher concentrations, the limited number of active sites on bio-chars could become saturated at a certain concentration, resulting in the very limited increment in adsorption capacity [33].

3.3. Adsorption mechanism

3.3.1. Kinetic studies

Adsorption rate constants for the MG were calculated by using the three mentioned kinetics in Table S2, which were used to describe the adsorption mechanism. As the adsorption kinetic parameters shown in Table S3, the relatively high R^2 values and the comparable theoretically calculated q_e values indicate that Pseudo-second-order model successfully described the kinetics of MG adsorption by bio-chars. The adsorption kinetic of the MG could probably be described by a pseudo second-order chemical reaction [35]. Generally, several adsorption steps involved in the adsorption dynamics: (i) the migration of the adsorbate molecules through the solution onto the surface of the adsorbent (film diffusion, or the boundary layer diffusion); (ii) the migration of the adsorbate molecules to the interior regions of the adsorbent (particle diffusion, or the intraparticle diffusion); and (iii) the sorption on the interior surfaces of the pores of the adsorbent (sorption). One or any combination of the three steps may be rate limiting [24,33]. Chemisorption (chemical reaction) may take place when the cationic MG could be involved by valency forces through sharing or the exchange of electrons between bio-char and MG [35].

The kinetic results were also analyzed and fitted to the Weber's the intra-particle diffusion model (Table S2) in order to elucidate the diffusion mechanism. Table S3 shows the C values (intercept) were not equal to zero, indicating the coexistence of external film and intra-particle diffusions during the adsorption process [36]. Fig. 4 indicates that the adsorption of MG followed three-step processes with the rapid initial adsorption controlled by the boundary layer diffusion (film diffusion) due to readily abundant and available active sites on the adsorbent surface; and with the period of the slower uptake being the intraparticle diffusion; and finally, with the equilibrium stage attained due to the saturated adsorption sites [33,36].

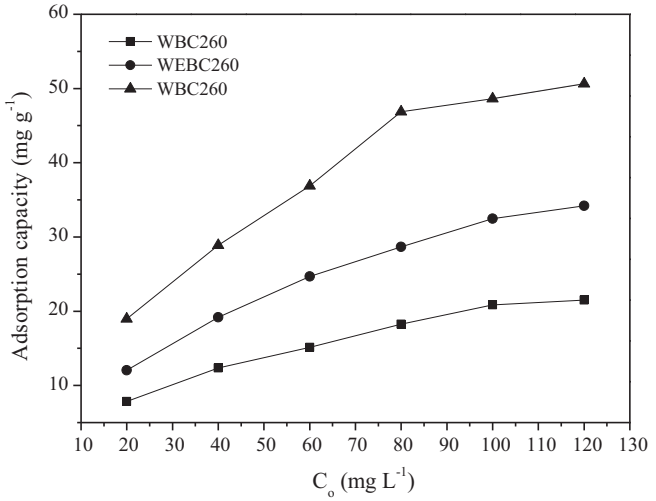

Fig. 5. The effect of initial adsorbate concentration on the adsorption of Malachite green by bio-chars (experimental conditions: adsorbent dose: 0.5 g L^{-1}, agitation speed: 150 rpm, pH: as received, temperature: 30 °C, contact time: 2.5 h).

3.3.2. Isotherm studies

The adsorption data of MG on bio-chars with different surface chemistry under various temperatures were fitted by using Langmuir, Freundlich, and Temkin models (expressed in Table S2). All these bio-chars can be well described by these three models as the parameters tabulated in Table S4 shown. The Langmuir model is a generally accepted model for the determination of theoretical specific area [24,37]. It can be found that the Langmuir isotherm had relatively higher correlation coefficient (R^2) than the other two isotherms, which indicates that the adsorption of MG on bio-chars was likely to be monolayer and that the distribution of active sites on the adsorbent was homogeneous [38,39].

Freundlich and Temkin models can also fit well with the experimental data. Table S4 displays that the values of heterogeneity factor n of Freundlich model were more than 1 for all bio-chars at different temperatures, indicating that the adsorption was favorable [24,39]. Note that Temkin adsorption isotherm considers chemical adsorption process (chemisorption) of an adsorbate onto the adsorbent [24]. The well fitness by Temkin model suggests that irreversible coulombic attraction and ion exchange might be the mechanism for MG adsorption by these liquefaction bio-chars [35]. It could be possible that coulombic attraction of MG (cationic) occurred due to the creation of a negative charge by the deprotonation of oxygen-containing functional groups like carboxylic groups on the bio-char surface [35].

Additionally, the MG adsorption capacities under temperatures of 30–60 °C increased against the increment of adsorption temperature (Fig. S5), indicating that increasing adsorption temperature favored the adsorption process.

Table 3
Thermodynamic parameters of Malachite green adsorption onto RH liquefaction bio-chars.

Sample	Temp. (°C)	ΔS^o (kJ mol^{-1} K^{-1})	ΔH^o (kJ mol^{-1})	ΔG^o (kJ mol^{-1})
WBC260	30	0.10	24.03	−7.39
	40			−8.67
	50			−9.23
	60			−10.67
WEBC260	30	0.16	40.71	−7.74
	40			−9.37
	50			−10.58
	60			−12.68
EBC260	30	0.18	44.38	−8.81
	40			−10.94
	50			−12.76
	60			−14.04

3.3.3. Thermaldynamic studies

In order to determine the thermodynamic adsorption behavior, the thermodynamic parameters – Gibbs free energy change (ΔG^o), enthalpy (ΔH^o), and entropy (ΔS^o) were estimated using equilibrium constants as a function of temperature related by Eqs. (8) and (9) expressed in Table S2. The slope and the intercept of plot between ln K_d and $1/T$ (Fig. S5) are used to evaluate ΔH^o and entropy ΔS^o, respectively. The adsorption process of MG by the liquefaction bio-chars were endothermic in nature as indicated by the positive values of ΔH^o [24,33] and verified by the fact that MG uptake increased with the increment of adsorption temperature (Fig. S5). The negative values of ΔG^o shown in Table 3 confirm the spontaneity of the adsorption of MG on these bio-chars and that the adsorption was more favorable with increasing temperature [24,33]. Moreover, the positive values of ΔS^o imply that the adsorption phenomenon was endothermic and the increment of randomness at the solid/solution interface increased during the adsorption process [24,36].

3.3.4. FT-IR studies

To understand the involvement of the functional groups on the bio-char surface, EBC260 before and after MG adsorption were examined by FT-IR spectroscopy (Fig. 6). The C=C stretching of the benzene ring on MG was supported by the peaks at 1475 and 1585 cm^{-1}. The aromatic tertiary amine and tertiary amine C—N stretching vibrations of MG corresponded to 1388 cm^{-1} and 1166 cm^{-1}, respectively [25]. As seen in Fig. 6, FT-IR spectra of MG loaded EBC260 showed some drastic differences when

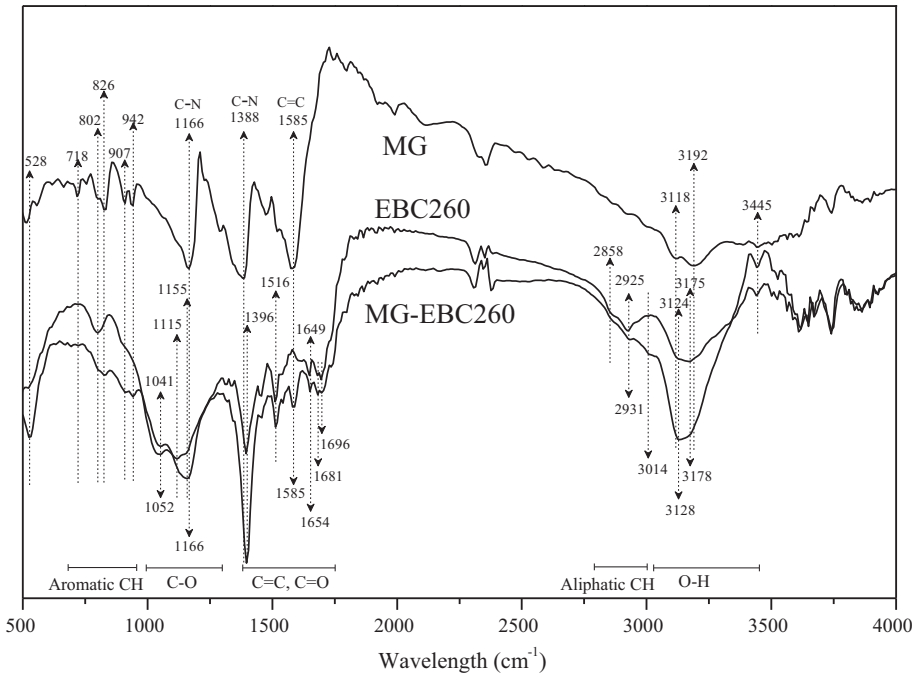

Fig. 6. Fourier transform infrared (FT-IR) spectra of E260 before and after the adsorption of Malachite green.

compared to the raw EBC260. The strengthened peaks at 1388 cm^{-1} (overlapped by the 1396 cm^{-1} peak of EBC260) and 1166 cm^{-1}, and the presence of peaks at 1585 cm^{-1} could well define the appearance or adsorption of MG on EBC260.

The MG adsorption mechanism may include electrostatic attraction, π-π interaction, and hydrogen bond, and also Van Der Waal attraction. Electrostatic attraction may probably be regarded as the main adsorption force note that bio-char was only effective on positively charged MG (Fig. 2) and MB (MB adsorption results were similar to those of MG as seen in Fig. S6) removal, but not on negatively charged MO (Fig. 2), and that the deprotonation of functional groups at higher pH resulted in the increment of adsorption capacity (Fig. 3). Additionally, the peaks at 1649 cm^{-1} and 1396 cm^{-1} corresponding to C═O and C—O of carboxylic groups slightly shifted (to 1654 cm^{-1}) and strengthened a lot, respectively (Fig. 6), which may be attributed to electrostatic attraction between negative charged carboxylate anion and positive charged MG [40]. Thus, carboxylic groups may be the most responsible electrostatic-attraction force donor for MG adsorption as also reported in Refs. [41,42]. Indeed, carboxylic groups favor MG adsorption as the net linear increase of MG uptake against the increment of the number of carboxylic groups indicated in Fig. S7.

In addition, the changes in peaks observed at 1115 cm^{-1}, 1649 cm^{-1}, and the band between 3100–3200 cm^{-1} were indicative of stretching vibration of C—O, C═O, and O—H bonds of carboxyl groups, which may due to the hydrogen bonding between carboxylic acids or their esters and MG [40]. Note that the peak at 1041 cm^{-1} corresponding to C—O of alcohols and/or phenolics slightly shifted to 1052 cm^{-1} and that O—H of hydroxyl groups (3100–3200 cm^{-1}) also shifted after adsorption of MG, the participation of hydroxyl groups (hydrogen bonding between hydroxyl groups and MG) would also exist during MG adsorption [40]. Finally, the changes of the peaks at 802 cm^{-1} (aromatic C—H), 2925 cm^{-1} (aliphatic C—H, shifted to 2931 cm^{-1}), and 1512 cm^{-1} (aromatic C═C, shifted to 1515 cm^{-1}) suggest the involvement of π–π interaction during MG adsorption [25].

4. Conclusions

The byproduct (bio-char) from liquefaction of rice husk displayed different surface chemistry in terms of the contents of oxygen-containing functional groups. WBC and WEBC were rich in phenolic groups and EBC was rich in carboxylic and lactonic groups. The MG adsorption capacities of the bio-chars depended strongly on the oxygen-containing functional groups especially carboxylic groups. Electrostatic attraction was believed to be the major adsorption mechanism. The MG adsorption kinetic can be fitted well by Pseudo-second-order model and the isotherm well described by Langmuir, Freundlich, and Temkin models. EBC (adsorption capacities of 32.5–67.6 mg g^{-1}) was more effective than WBC and WEBC on MG removal from aqueous solution when the adsorbent was used as received (without pH adjustment). Note that both the bio-oil and bio-char yields with ethanol as the solvent were high [12], ethanol would be more feasible for both bio-oil and bio-char production than water or water/ethanol mixture in liquefaction.

Acknowledgments

The authors gratefully acknowledge the financial support provided by the National Natural Science Foundation of China, China (Nos. 21276069 and 71431006), the Specialized Research Fund for the Doctoral Program of Higher Education, China (No. 20120161130002), and the Collaborative Innovation Center of Resource-conserving & Environment-friendly Society and Ecological Civilization, China.

Appendix A. Supplementary material

Supplementary data associated with this article can be found, in the online version, at http://dx.doi.org/10.1016/j.fuel.2015.04.019.

References

[1] Lee YH, Pavlostathis SG. Decolorization and toxicity of reactive anthraquinone textile dyes under methanogenic conditions. Water Res 2004;38:1838–52.
[2] Yagub MT, Sen TK, Afroze S, Ang HM. Dye and its removal from aqueous solution by adsorption: a review. Adv Colloid Interface Sci 2014;209:172–84.
[3] Salleh MAM, Mahmoud DK, Karim WAWA, Idris A. Cationic and anionic dye adsorption by agricultural solid wastes: a comprehensive review. Desalination 2011;280:1–13.
[4] Chen Y, Zhu Y, Wang Z, Li Y, Wang L, Ding L, et al. Application studies of activated carbon derived from rice husks produced by chemical-thermal process–a review. Adv Colloid Interface Sci 2011;163:39–52.
[5] Nguyen TAH, Ngo HH, Guo WS, Zhang J, Liang S, Yue QY, et al. Applicability of agricultural waste and by-products for adsorptive removal of heavy metals from wastewater. Bioresour Technol 2013;148:574–85.
[6] Chuah TG, Jumasiah A, Azni I, Katayon S, Thomas Choong SY. Rice husk as a potentially low-cost biosorbent for heavy metal and dye removal: an overview. Desalination 2005;175:305–16.
[7] Rahman Ia, Saad B, Shaidan S, Sya Rizal ES. Adsorption characteristics of malachite green on activated carbon derived from rice husks produced by chemical–thermal process. Bioresour Technol 2005;96:1578–83.
[8] Guo Y, Zhang H, Tao N, Liu Y, Qi J, Wang Z, et al. Adsorption of malachite green and iodine on rice husk-based porous carbon. Mater Chem Phys 2003;82:107–15.
[9] Agrafioti E, Kalderis D, Diamadopoulos E. Arsenic and chromium removal from water using biochars derived from rice husk, organic solid wastes and sewage sludge. J Environ Manage 2014;133:309–14.
[10] Liu Z, Zhang F-S. Removal of lead from water using biochars prepared from hydrothermal liquefaction of biomass. J Hazard Mater 2009;167:933–9.
[11] Liu Z, Zhang F-S, Wu J. Characterization and application of chars produced from pinewood pyrolysis and hydrothermal treatment. Fuel 2010;89:510–4.
[12] Liu Y, Yuan X, Huang H, Wang X, Wang H, Zeng G. Thermochemical liquefaction of rice husk for bio-oil production in mixed solvent (ethanol–water). Fuel Process Technol 2013;112:93–9.
[13] Liu Z, Zhang F-S. Removal of copper (II) and phenol from aqueous solution using porous carbons derived from hydrothermal chars. Desalination 2011;267:101–6.
[14] Leng L, Yuan X, Huang H, Wang H, Wu Z, Fu L, et al. Characterization and application of bio-chars from liquefaction of microalgae, lignocellulosic biomass and sewage sludge. Fuel Process Technol 2015;129:8–14.
[15] Smith KM, Fowler GD, Pullket S, Graham NJD. Sewage sludge-based adsorbents: a review of their production, properties and use in water treatment applications. Water Res 2009;43:2569–94.
[16] Zhu X, Liu Y, Zhou C, Luo G, Zhang S, Chen J. A novel porous carbon derived from hydrothermal carbon for efficient adsorption of tetracycline. Carbon N Y 2014;77:627–36.
[17] Boehm HP. Some aspects of the surface chemistry. Carbon N Y 1994;32:759–69.
[18] Boehm HP. Surface oxides on carbon and their analysis: a critical assessment. Carbon N Y 2002;40:145–9.
[19] Chun Y, Sheng G, Chiou CT, Xing B. Compositions and sorptive properties of crop residue-derived chars. Environ Sci Technol 2004;38:4649–55.
[20] Parthasarathy P, Narayanana KS, Arockiam L. Study on kinetic parameters of different biomass samples using thermo-gravimetric analysis.pdf. Biomass Bioenergy 2013;58:1–9.
[21] Huang H, Yuan X, Zeng G, Wang J, Li H, Zhou C, et al. Thermochemical liquefaction characteristics of microalgae in sub- and supercritical ethanol. Fuel Process Technol 2011;92:147–53.
[22] Huang H, Yuan X, Zeng G, Liu Y, Li H, Yin J, et al. Thermochemical liquefaction of rice husk for bio-oil production with sub- and supercritical ethanol as solvent. J Anal Appl Pyrolysis 2013;102:60–7.
[23] Chen Y, Zhai S, Liu N, Song Y, An Q, Song X. Dye removal of activated carbons prepared from NaOH-pretreated rice husks by low-temperature solution-processed carbonization and H3PO4 activation. Bioresour Technol 2013;144:401–9.
[24] Salima A, Benaouda B, Noureddine B, Duclaux L. Application of *Ulva lactuca* and *Systoceira stricta* algae-based activated carbons to hazardous cationic dyes removal from industrial effluents. Water Res 2013;47:3375–88.
[25] Wu Z, Zhong H, Yuan X, Wang H. Adsorptive removal of methylene blue by rhamnolipid-functionalized graphene oxide from wastewater. Water Res 2014;67:330–44.
[26] Xiao X, Chen B, Zhu L. Transformation, morphology, and dissolution of silicon and carbon in rice straw-derived biochars under different pyrolytic temperatures. Environ Sci Technol 2014;48:3411–9.
[27] Daifullah AAM, Girgis BS, Gad HMH. Utilization of agro-residues (rice husk) in small waste water treatment plans. Mater Lett 2003;57:1723–31.
[28] Al-Ghouti MA, Hawari A, Khraisheh M. A solid-phase extractant based on microemulsion modified date pits for toxic pollutants.pdf. J Environ Manage 2013;130:80–9.

[29] Lu H, Zhang W, Yang Y, Huang X, Wang S, Qiu R. Relative distribution of Pb2+ sorption mechanisms by sludge-derived biochar. Water Res 2012;46:854–62.
[30] Wang S, Zhu ZH, Coomes A, Haghseresht F, Lu GQ. The physical and surface chemical characteristics of activated carbons and the adsorption of methylene blue from wastewater. J Colloid Interface Sci 2005;284:440–6.
[31] Zhou Y, Zhang M, Hu X, Wang X, Niu J, Ma T. Adsorption of cationic dyes on a cellulose-based multicarboxyl adsorbent. J Chem Eng Data 2013;58:413–21.
[32] Lee Y-C, Kim J-Y, Shin H-J. Removal of Malachite Green (MG) from aqueous solutions by adsorption, precipitation, and alkaline fading using talc. Sep Sci Technol 2013;48:1093–101.
[33] Saha P, Chowdhury S, Gupta S, Kumar I. Insight into adsorption equilibrium, kinetics and thermodynamics of Malachite Green onto clayey soil of Indian origin. Chem Eng J 2010;165:874–82.
[34] Wang S, Zhu Z. Effects of acidic treatment of activated carbons on dye adsorption. Dye Pigment 2007;75:306–14.
[35] Bulut E, Özacar M, Şengil İA. Adsorption of malachite green onto bentonite: equilibrium and kinetic studies and process design. Microporous Mesoporous Mater 2008;115:234–46.
[36] Wang H, Yuan X, Zeng G, Leng L, Peng X, Liao K, et al. Removal of malachite green dye from wastewater by different organic acid-modified natural adsorbent: kinetics, equilibriums, mechanisms, practical application, and disposal of dye-loaded adsorbent. Environ Sci Pollut Res Int 2014;21:11552–64.
[37] El QadaEN, Allen SJ, Walker GM. Adsorption of Methylene Blue onto activated carbon produced from steam activated bituminous coal: a study of equilibrium adsorption isotherm. Chem Eng J 2006;124:103–10.
[38] Ling C, Liu F-Q, Xu C, Chen T-P, Li A-M. An integrative technique based on synergistic coremoval and sequential recovery of copper and tetracycline with dual-functional chelating resin: roles of amine and carboxyl groups. ACS Appl Mater Interfaces 2013;5:11808–17.
[39] Kong J, Yue Q, Sun S, Gao B, Kan Y, Li Q, et al. Adsorption of Pb(II) from aqueous solution using keratin waste – hide waste: equilibrium, kinetic and thermodynamic modeling studies. Chem Eng J 2014;241:393–400.
[40] Wahab MA, Jellali S, Jedidi N. Ammonium biosorption onto sawdust: FTIR analysis, kinetics and adsorption isotherms modeling. Bioresour Technol 2010;101:5070–5.
[41] Sharma P, Das MR. Removal of a cationic dye from aqueous solution using graphene oxide nanosheets: investigation of adsorption parameters. J Chem Eng Data 2013;58:151–8.
[42] Sarkar AK, Pal A, Ghorai S, Mandre NR, Pal S. Efficient removal of malachite green dye using biodegradable graft copolymer derived from amylopectin and poly(acrylic acid). Carbohydr Polym 2014;111:108–15.